Received: 16 January 2020 | Revised: 22 October 2020 | Accepted: 22 October 2020

DOI: 10.1002/glia.23934

GLIA

WILEY

RESEARCH ARTICLE

Neuronal brain-derived neurotrophic factor manipulates microglial dynamics

Junya Onodera[1] | Hidetaka Nagata[2] | Ai Nakashima[1] | Yuji Ikegaya[1] | Ryuta Koyama[1]

[1]Laboratory of Chemical Pharmacology, Graduate School of Pharmaceutical Sciences, The University of Tokyo, Tokyo, Japan

[2]Platform Technology Research Unit, Sumitomo Dainippon Pharma Co., Ltd., Osaka, Japan

Correspondence
Ryuta Koyama, Laboratory of Chemical Pharmacology, Graduate School of Pharmaceutical Sciences, The University of Tokyo, 7-3-1 Hongo, Bunkyo-ku, Tokyo 113-0033, Japan.
Email: rkoyama@mol.f.u-tokyo.ac.jp

Funding information
Japan Science and Technology Agency, Grant/Award Numbers: JPMJER1801, JPMJPR18H4; Japan Society for the Promotion of Science, Grant/Award Number: 17H03988

Abstract

Brain-derived neurotrophic factor (BDNF), a main member of the neurotrophin family that is active in the brain, supports neuronal survival and growth. Microglial BDNF affects both the structural and functional properties of neurons. In contrast, whether and how neuronal BDNF affects microglial dynamics remain largely undetermined. Here, we examined the effects of BDNF on the properties of microglia in the CA3 region of the hippocampus. We chose this site because the axonal boutons of hippocampal mossy fibers, which are mostly formed in the CA3 region, contain the highest levels of BDNF in the rodent brain. We transfected mouse dentate granule cells with an adeno-associated virus that encodes both a BDNF short hairpin RNA (shRNA) and red fluorescent protein to examine the effects of mossy fiber-derived BDNF on microglia. Based on immunohistochemistry, BDNF knockdown with an shRNA resulted in an increase in microglial density in the mossy fiber pathway and increased engulfment of mossy fiber axons by microglia. In addition, we performed time-lapse imaging of microglial processes in hippocampal slice cultures to examine the effects of BDNF on microglial motility. Time-lapse imaging revealed increases in the motility of microglial processes and the engulfment of mossy fiber synapses by microglia when BDNF signaling was pharmacologically blocked. Thus, neuronal BDNF prevents microglia from engulfing mossy fiber synapses in the hippocampus.

KEYWORDS

BDNF, hippocampus, microglia, neuroplasticity, phagocytosis

1 | INTRODUCTION

Microglia are brain-resident immune cells that monitor the brain parenchyma with highly motile processes that dynamically interact with other brain cells, including other microglia. Several mechanisms mediated by either soluble or contact-dependent factors (Wohleb, 2016) have been shown to modulate neuron–microglia interactions. Some studies have reported a role for brain-derived neurotrophic factor (BDNF) in neuron–microglia interactions. Dimerized BDNF binds to its receptors, tropomyosin-related kinase B (TrkB), a tyrosine kinase receptor, and the p75 neurotrophin receptor ($p75^{NTR}$), affecting the electrophysiological and morphological properties of neurons, as well as their survival (Korte et al., 1995; Lindholm, Carroll, Tzimagiorgis, & Thoenen, 1996; Wang et al., 2015). Microglia express BDNF, and microglial-derived BDNF affects neuronal structure and function. According to Parkhurst et al. (2013), microglial BDNF affects synaptic plasticity. In addition, in the study by Coull et al., microglial BDNF caused a shift in the neuronal anion gradient in a neuropathic pain model (Coull et al., 2005). The neuron–microglia interactions mediated by microglial BDNF have been extensively studied (Ferrini & De Koninck, 2013). In contrast, whether and how neuronal BDNF affects microglial dynamics have not been reported. Furthermore,

controversy exists regarding whether microglia express the BDNF receptor TrkB. Some studies have reported that microglia express TrkB (Zhang et al., 2003), while other studies did not observe BDNF expression in microglia (Frisen et al., 1993). These different outcomes may result from microglial heterogeneity in animals of different ages and in the brain region of interest.

We focused on neuron–microglia interactions in the CA3 region of the hippocampus to directly examine whether neuronal BDNF affects microglial dynamics. We chose this region because the axonal boutons of mossy fibers, which are the axons of dentate granule cells that form synapses on the dendrites of CA3 pyramidal neurons, contain the highest levels of BDNF in the rodent brain (Conner, Lauterborn, Yan, Gall, & Varon, 1997), thus allowing us to efficiently assess the effects of axonal BDNF on microglial dynamics. Hippocampal BDNF levels fluctuate in response to some pathological conditions. The expression of the BDNF mRNA and protein, which are expressed in a neuronal activity-dependent manner, was reported to be elevated in the hippocampus of patients with epilepsy (Murray et al., 2000; Palomer, Carretero, Benveqnu, Dotti, & Martin, 2016; Takahashi et al., 1999). On the other hand, stress decreases BDNF expression in the hippocampus, where receptors for glucocorticoid, the major stress reactive adrenal steroid, are expressed at high levels (Duman & Monteggia, 2006). In these cases, the properties of hippocampal microglia are altered. The properties of microglia are altered in subjects with epilepsy and depression (Hiragi, Ikegaya, & Koyama, 2018; Ménard, Hodes, & Russo, 2016). Therefore, the hippocampus is a suitable target brain region to study the effects of BDNF on microglia, not only from the experimental perspective, that is, high levels of BDNF are present in mossy fiber boutons, but also from a clinical perspective.

Here, we investigated whether and how BDNF affects microglial dynamics in the hippocampal CA3 region primarily using shRNA-mediated suppression of BDNF expression in dentate granule cells. Microglia phagocytose or trogocytose axonal compartments to refine neuronal circuits (Schafer et al., 2012; Weinhard et al., 2018); these functions of microglia crucially depend on the surveillance and detection of neuronal components mediated by extracellular molecules (Madry & Attwell, 2015). Thus, we focused on the effects of BDNF on microglial dynamics, such as density, motility, and the ability to engulf neuronal components.

2 | MATERIALS AND METHODS

2.1 | Animals

Experiments were performed with the approval of the Animal Experiment Ethics Committee at the University of Tokyo (approval numbers: P24-10 and P24-15) and in accordance with the University of Tokyo guidelines for the care and use of laboratory animals.

Female C57BL/6J mice (SLC Japan Inc., Japan; RRID: IMSR_JAX: 000664) and male CX3CR1$^{GFP/GFP}$ mice (Jackson Labs, Farmington, CT; Stock No: 005582; C57BL/6 genetic background) were housed in cages under standard laboratory conditions (12 hr light/dark cycle, free access to food and water). Male CX3CR1$^{GFP/GFP}$ mice were crossed with female C57BL/6J mice to obtain CX3CR1$^{GFP/+}$ mice. All efforts were made to minimize the animals' suffering and the number of animals used.

2.2 | Viral vector production

Viral vectors were packaged in three plasmids. Each plasmid expressed the adeno-associated virus (AAV)2 replicase, AAV-DJ capsid protein, or adenovirus helper proteins (pHelper; Agilent, Santa Clara, CA). The plasmids were cotransfected into AAV-293 cells (Agilent) at a molar ratio of 1:1:1. In a transfer plasmid, short hairpin RNAs (shRNA) were inserted between the mouse CaMKIIα promoter, mCherry, and bGH polyA. The expression of the shRNA was under the control of the Pol III murine U6 promoter. The target regions of the shRNA sequences were as follows: BDNF shRNA #1, 5′-CTCTTTCTGCTGGAGGAATAC-3′; BDNF shRNA #2, 5′-GCATGCTGCTTTAATTGTGAA-3′; and BDNF shRNA #3, 5′-AAAGTCTTGCTGTGGTCTCTT-3′. A negative control shRNA, 5′-TGGTTTACATGTCGACTAA-3′, which has been previously reported (Samad et al., 2013), was used in the current study. All rAAV vectors were prepared using the adenovirus-free triple-plasmid transfection system and the purification method previously reported by Matsushita et al. (1998). Viral vectors were stored at −80°C, and the genomic titer of each virus was determined using quantitative PCR.

2.3 | Stereotaxic surgery for AAV injection

Eight-week-old C57BL/6J mice were injected with rAAV-DJ (mCamKIIα)mCherry_shBDNF or rAAV-DJ(mCamKIIα)mCherry_shcontrol using the method described below. Mice were anesthetized with pentobarbital (2.5 mg/kg, intraperitoneal [i.p.] injection) and xylazine (10 mg/kg, i.p. injection) and then placed in a stereotaxic apparatus. The virus (1 μl per side) was injected into the bilateral dentate gyrus (AP: −2 mm, LM: ±1.3 mm, DV: −2.2 mm) at a rate of 0.25 μl/min using glass pipettes. Glass pipettes were then left in place for a few minutes and slowly withdrawn.

2.4 | Seizure induction

Four weeks after stereotaxic surgery, kainic acid (Sigma, St. Louis, MO) was injected (i.p.) into C57BL/6J mice to induce seizures. The severity of kainic acid-induced seizures was scored using Racine's scale with some modifications (Racine, 1972): Stage 1, freezing behavior; Stage 2, rigid posture with a straight and rigid tail; Stage 3, repetitive head bobbing and rearing into a sitting position with shaking forelimbs; Stage 4, rearing and falling, jumping, and running with a period of total stillness; Stage 5, continuous Stage 4 behaviors; and

Stage 6, loss of posture and generalized convulsion activity, usually preceding death.

After the first kainic acid injection (10 mg/kg, i.p.), mice progressed through the different seizure stages. An additional injection of kainic acid (5 mg/kg, i.p.) was administered to mice that failed to reach Stage 4 seizures within 30 min of the first injection.

Mice were anesthetized as described above and perfused 3 hr after reaching Stage 4 or higher. Control mice received a saline injection (i.p.) and exhibited no abnormal behaviors.

2.5 | Organotypic hippocampal slice culture

Brains from postnatal Day 10 (P10) mice were sectioned into 400-μm thick horizontal slices using a DTK-1500 slicer (Dosaka EM, Kyoto, Japan) in aerated, ice-cold Gey's balanced salt solution containing 25 mM glucose. The hippocampal regions of each slice were dissected and incubated for 30–90 min at 4°C in incubation medium composed of minimal essential medium (MEM), 9.0 mM Tris, 22.9 mM HEPES, and 63.1 mM glucose supplemented with penicillin and streptomycin. Next, the slices were placed on Omnipore membrane filters (JHWP02500; Millipore, Bedford, MA) in doughnut plates (Hazai-Ya, Tokyo, Japan; Koyama et al., 2007) and incubated with culture medium containing 50% MEM, 25% horse serum (26050-088; heat-inactivated and filter-sterilized; Gibco, Grand Island, NY), 25% Hank's balanced salt solution, 6.6 mM Tris, 16.9 mM HEPES, 4.0 mM $NaHCO_3$, 29.8 mM glucose, and a 1% gentamicin sulfate solution (16672-04; Nacalai, Kyoto, Japan). Finally, the slices were cultured at 35°C in a humidified incubator with 5% CO_2 and 95% air. The culture medium was changed twice weekly.

2.6 | Live imaging of microglia in hippocampal slice cultures

Live imaging of microglia in hippocampal slice cultures was performed at 9 days in vitro (9 DIV) using an FV1000 scanning confocal microscope (Olympus, Tokyo, Japan). The imaging chamber (Tokai Hit, Shizuoka, Japan) was maintained at 35°C with 5% CO_2 starting 1 hr before live imaging. Hippocampal slices with membrane filters were gently placed in 35 mm dishes filled with culture medium, and the dishes were placed in the imaging chamber. For all imaging sessions, we set a region of interest containing several microglia in the CA3 region at a depth of 10 μm from the slice surface. The slice was treated with 0.1% DMSO (Nacalai Tesque), 1.6 μg/ml mouse anti-BDNF antibody (#AB1779SP, Millipore), 1.6 μg/ml heat-inactivated anti-BDNF antibody, 0.3 μM K252a (Wako) or 100 μM TAT-Pep5 (Millipore) immediately prior to live imaging. The heat-inactivated anti-BDNF antibody was prepared by boiling the stock solution of the anti-BDNF antibody at 100°C for 15 min, as described in a previous study (Crozier, Bi, Han, & Plummer, 2008). Immediately after the application of BDNF signaling inhibitors, fluorescence images of green fluorescent protein (GFP) fluorescence were captured, and *Z*-series images (10 sections) were acquired at a rate of 1 frame/min for an hour with a ×40 water-immersion objective at a voxel size of 0.311–0.311–1.00 μm (x–y–z).

2.7 | Analysis of microglial motility

GFP signals of *Z*-stack images were used to analyze the microglial process motility and surveillance areas. We applied a threshold to GFP signals that would not mask thin processes to distinguish the signals of microglial processes from background noise. The *Z*-stack images were flattened into a maximum-intensity projection using ImageJ software (NIH, Bethesda, MD).

The process length was measured every minute for 10 min, as shown in Figure 4. The length of the microglial process was defined as the length of a line segment connecting the starting point and the end point of a microglial process; the starting point was set as a point of the microglial process emanating from the soma, and the end point was set at the tip of the microglial process furthest from the soma.

The microglial surveillance area was measured every minute for 30 min, as shown in Figure 5. For the analysis of "surveillance area expansion and retraction" and "total surveillance area," threshold datasets of 31 consecutive images that contained only one microglial cell were used. Surveillance area expansion and retraction were defined as areas where the GFP signal appeared or disappeared, respectively, compared with the image captured in the previous minute. Initially, 2 datasets of 30 consecutive images (one dataset included 30 images from 1st to 30th minutes and the other dataset included images from the 2nd to 31st minutes) were generated from the threshold datasets to analyze these parameters. Next, by using the subtraction operation of the Image calculator in ImageJ, one dataset was subtracted from the other dataset and vice versa to generate two datasets of surveillance area expansion and retraction. Finally, the average surveillance area expansion and retraction per minute were calculated from these datasets. The total surveillance area was defined as the area where the GFP signal appeared or disappeared even once within 30 min (images were captured every minute). For the analysis, the image of the average GFP signal intensity for each pixel of the threshold data was generated using the Z-projection feature in ImageJ. Then, the area where the signal intensity was neither the minimum nor maximum in the image was regarded as the total surveillance area, and the area was calculated. Pseudocolor images of the average GFP signal intensity (microglia stability) are shown in Figure 5d.

2.8 | Sample preparation and immunohistochemistry

Mice were anesthetized with isoflurane and perfused transcardially with cold phosphate-buffered saline (PBS) followed by 4% paraformaldehyde (PFA). Brain samples were postfixed with 4% PFA for 24 hr at 4°C. Coronal hippocampal sections (100 μm) were prepared using a

vibratome (Dosaka EM). Slices were then permeabilized for 40 min at room temperature in 0.1 M phosphate buffer containing 0.3% Triton X-100 and 10% goat serum. Samples were subsequently incubated with primary antibodies in 0.1 M phosphate buffer containing 0.3% Triton X-100 and 10% goat serum overnight on ice with agitation. After rinses with 0.1 M phosphate buffer, the samples were incubated with secondary antibodies in 0.1 M phosphate buffer containing 10% goat serum for 24 hr on ice with agitation. The primary antibodies used in this study were mouse anti-mCherry (1:1,000; Abcam, Cambridge, UK), rabbit anti-Ki67 (1:500; Abcam), rabbit anti-Iba1 (1:500; Wako, Osaka, Japan), rabbit anti-SPO (1:500; Synaptic Systems, Göttingen, Germany), guinea pig anti-Iba1 (1:500; Synaptic Systems), rat anti-CD68 (1:500; AbD Serotex, Oxford, UK), mouse anti-p-Trk (1:20; Santa Cruz, Dallas, TX), mouse anti-proBDNF (1:50; Santa Cruz), and rabbit anti-cleaved caspase-3 (Cell Signaling Technology, Danvers, MA). Secondary antibodies conjugated with Alexa Fluor dyes (1:500; Invitrogen, Gaithersburg, MD) were used. After an overnight incubation at 4°C with a secondary antibody, sections were incubated with Hoechst 33342 (1:1,000; Invitrogen) for 10 min to visualize nuclei.

Cultured slices were fixed with 4% PFA at 4°C for 24 hr. Fixed samples were rinsed three times with PBS. Slices were then permeabilized with 0.1 M phosphate buffer containing 0.3% Triton X-100 and 10% goat serum for 40 min at room temperature. Samples were subsequently incubated with primary antibodies in 0.1 M phosphate buffer containing 0.3% Triton X-100 and 10% goat serum for 48 hr on ice with agitation. After rinses with 0.1 M phosphate buffer, the samples were incubated with secondary antibodies in 0.1 M phosphate buffer containing 10% goat serum for 24 hr on ice with agitation. The primary antibodies used in this study were chicken anti-GFP (1:1,000; Abcam), rabbit anti-SPO (1:500; Synaptic Systems), and rat anti-CD68 (1:500; AbD Serotex). Secondary antibodies conjugated with Alexa Fluor dyes (1:500; Invitrogen) were used. After an overnight incubation at 4°C with the secondary antibody, sections were incubated with Hoechst 33342 (1:1,000; Invitrogen) for 10 min.

2.9 | Image analysis

Images were acquired with an FV1000 scanning confocal microscope (Olympus) equipped with diode lasers (405, 473, 559, and 635 nm) and analyzed using ImageJ software (NIH). *Z*-series images (six sections) were acquired with a ×20 objective at a voxel size of 0.621–0.621–1.00 μm (x–y–z) to analyze the colocalization of Hoechst and cleaved caspase-3 staining. For the analysis of microglial density, *Z*-series images (11 sections) were acquired with a ×20 objective at a voxel size of 0.621–0.621–1.00 μm (x–y–z). For the analysis of microglial engulfment, *Z*-series images (10 sections) were acquired with a ×60 objective at a voxel size of 0.207–0.207–0.500 μm (x–y–z). For the analysis of proBDNF and microglial levels of phosphorylated Trk (p-Trk) in SL, *Z*-series images (four sections) were acquired with a ×100 objective at a voxel size of 0.124–0.124–0.333 μm (x–y–z).

The quantification of the CD68 and p-Trk volume and engulfed mCherry and SPO volume was performed using a previously described method, with minor modifications (Schafer et al., 2012). The intensities of Iba1, CD68, p-Trk, mCherry, and SPO immunofluorescence staining were detected by determining the threshold of the fluorescence intensities using ImageJ software. Then, images showing the colocalization of Iba1 and CD68 or p-Trk were prepared, and the extent of the colocalization was measured in the stratum lucidum (SL). Images showing the colocalization of internalized CD68 in microglia and mCherry or SPO were prepared, and the extent of the colocalization was measured in the SL to determine the amount of mCherry or SPO engulfed by microglia.

2.10 | Statistical analysis

Data were pooled from at least three independent experiments and are presented as plots with lines indicating the means ± *SD* or *SEM*, or as box and whisker plots showing the distributions and medians (solid line) of the data (box edges indicate 25th and 75th percentiles; whiskers indicate minimum and maximum values). Data were collected and statistically analyzed by two independent researchers in a blinded manner. The Mann–Whitney *U* test was used for nonparametric statistics, while Student's *t* test or Dunnett's test was performed after one-way analysis of variance (ANOVA) for parametric statistics. All statistical analyses were performed using Prism 6.0 software (GraphPad, San Diego, CA).

3 | RESULTS

3.1 | BDNF knockdown in dentate granule cells

BDNF is abundant in the hippocampus and particularly in the axonal boutons of dentate granule cells, that is, the hippocampal mossy fiber boutons (Conner et al., 1997; Danzer & McNamara, 2004), as BDNF is released from the presynaptic boutons (Li, Calfa, Inoue, Amaral, & Pozzo-Miller, 2010). Thus, the mossy fiber pathway in the SL of the hippocampal CA3 region is the appropriate region of the brain to study the role of neuronal BDNF in neuron–microglia interactions (Figure 1). We injected rAAV-DJ(mCamKIIα)-mCherry-shBDNF or AAVs encoding the control shRNA into the dentate gyrus of adult mice to knockdown BDNF expression in the mossy fibers (Figure 1a). Mice were sacrificed 4 weeks after the virus injection, and brain sections were immunostained to examine the localization of mCherry. Based on the immunohistochemical staining, mCherry expression was mainly restricted to the hippocampal mossy fiber pathway in the SL (Figure 1a,b). In the SL, approximately 30% of synaptoporin (SPO), a mossy fiber presynaptic marker (Andoh et al., 2019; Williams et al., 2011), was colocalized with mCherry-positive mossy fiber boutons (Figures 1c and S1). We confirmed neuronal BDNF knockdown in the SL by the reduction in the signal for proBDNF, a BDNF precursor protein, which was previously used to confirm the

expression of BDNF (Falcicchia et al., 2016). The images of immunostaining revealed decreased proBDNF levels in the SL, including the mossy fiber boutons (Figure 1d,e). Together with the findings of previous studies showing that BDNF expression is mainly localized in boutons (Conner et al., 1997; Danzer & McNamara, 2004), our results indirectly reflect the reduction of BDNF in mossy fiber boutons

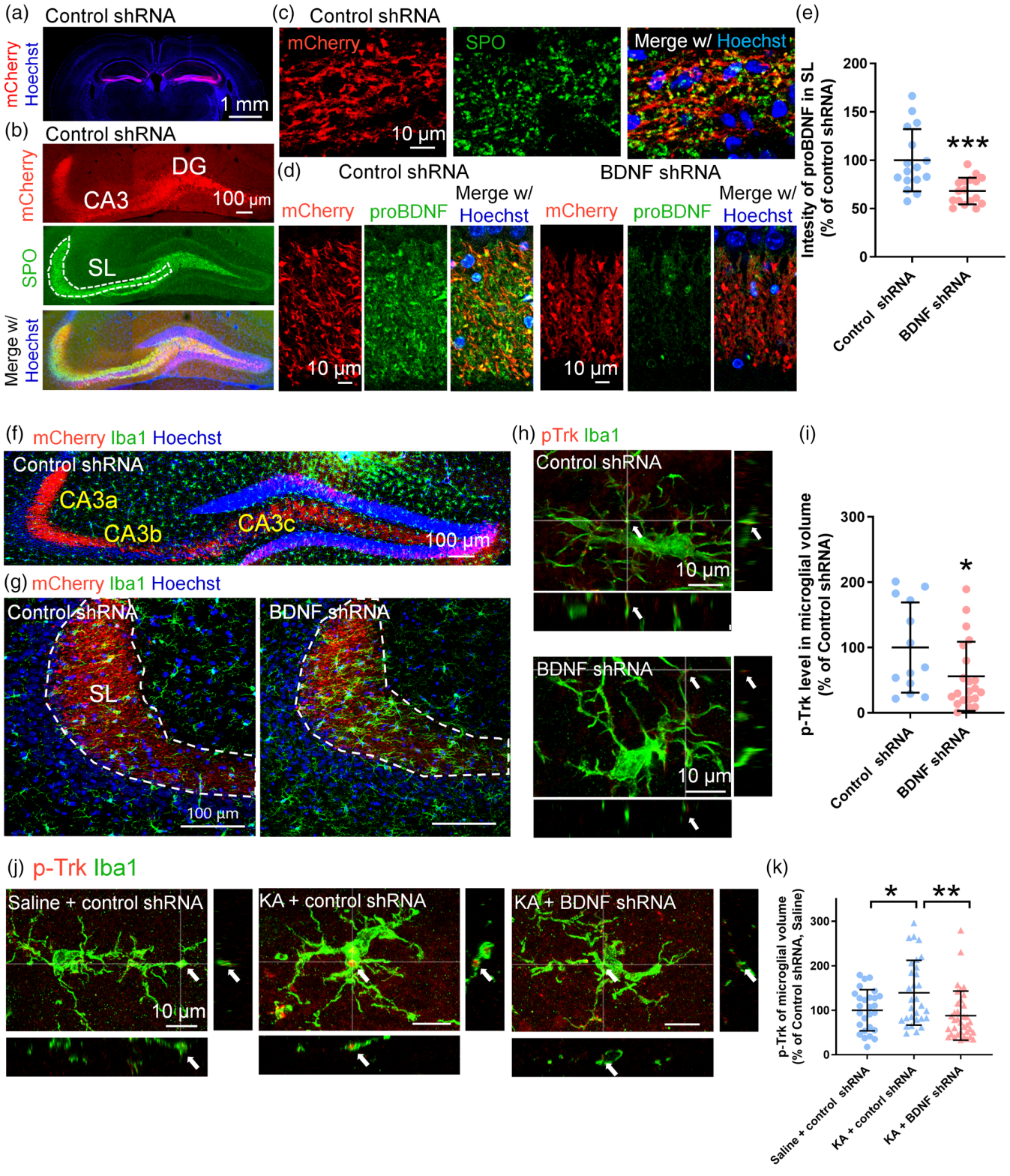

FIGURE 1 Legend on next page.

induced by the BDNF shRNA. Although BDNF regulates neuronal survival (Lindholm et al., 1996), we confirmed that BDNF knockdown did not induce significant neuronal death by measuring the density of cleaved caspase 3-positive and -negative cells in the dentate granule cell and CA3 pyramidal cell populations (Figure S2).

We focused on the SL in hippocampal CA3a and CA3b regions, which contains few axons of mossy cells (Lübke, Frotscher, & Spruston, 1998), to investigate the effect of mossy fiber-derived BDNF on microglia (Figure 1f,g). We examined whether mossy fiber-derived BDNF induced the phosphorylation of the BDNF receptor Trk (p-Trk) in microglia located in the SL (Figure 1h,i). Immunohistochemical staining for the colocalization of p-Trk and the microglial marker Iba1 revealed that the microglial p-Trk level was decreased following the knockdown of neuronal BDNF, suggesting that neuronal BDNF tonically activates microglial Trk receptors (Figure 1h,i). Next, we investigated whether an increase in neuronal BDNF expression led to an increase in microglial p-Trk levels. For this purpose, we treated mice with kainic acid, a treatment that has been shown to induce the activity-dependent release of BDNF from mossy fibers and subsequent phosphorylation of TrkB in the SL (Helgager, Liu, & McNamara, 2013), 4 weeks after the virus injection. The microglial p-Trk level was increased following kainic acid administration; this increase was blocked in mice injected with an AAV encoding the BDNF shRNA (Figure 1j,k). Based on these results, microglia in the SL possess functional Trk receptors, consistent with a previous report (Ding et al., 2020). Notably, the experiments using KA described above do not confirm that the phosphorylation of TrkB was induced in microglia by mossy fiber-derived BDNF because KA-induced seizures induce various responses, including excess activation of mossy fibers and neuron-to-astrocyte and neuron-to-microglia communication.

3.2 | Mossy fiber-derived BDNF modulated the microglial density and engulfment of axons in the SL

We investigated whether knockdown of BDNF in mossy fibers affected the distribution of microglia in the SL. First, we examined whether the microglial density was altered 4 weeks after the virus injection in the SL and areas adjacent to the SL, including the stratum radiatum (SR), stratum pyramidale (SP), and stratus oriens (SO) (Figure 2a). The microglial density was not significantly different between the control shRNA and BDNF shRNA groups in each area, except the SL (Figure 2b–e). We also confirmed that the volume of the SL was not altered upon BDNF knockdown (Figure 2f).

Next, we examined the time point when the microglial density in the SL started to increase. For this purpose, we performed immunohistochemical staining 2 weeks after the virus injection (Figure S3), and observed a trend of an increase in the microglial density following neuronal BDNF knockdown. However, the increase was not statistically significant, suggesting that at least 2 weeks after the virus injection were required to achieve an increase in microglial density.

Because the density of microglia was not changed in areas adjacent to the SL, we suspected that the frequency of microglial proliferation, but not microglial migration, contributed to the increased microglial density in the SL. We immunostained slices with an antibody against the Ki67 protein, a cellular marker for proliferation, 1 week after the virus injection to assess this possibility. BDNF knockdown resulted in an increase in the Ki67-positive microglial density in the SL (Figure 2g,k). Thus, microglial proliferation contributes to the increase in the microglial density.

Next, we investigated whether BDNF knockdown in mossy fibers affected the microglial phagocytic capacity in the SL at 4 weeks after the virus injection. We immunohistochemically examined the volume of CD68 in microglia and the volume of mCherry engulfed in CD68-positive lysosomes when BDNF was knocked down (Figure 3a). CD68 is a lysosomal protein associated with the phagocytic activity of microglia (Perego, Fumagalli, & de Simoni, 2011). The volume of CD68 in the microglia was unchanged, while the volume of total CD68 in the SL was increased upon BDNF knockdown, suggesting that the total phagocytic activity of microglia in the SL was increased (Figure 3b,d). Consistent with these results, we confirmed that the volume of engulfed mCherry in the microglia was not changed, while the volume of total engulfed mCherry was increased upon BDNF knockdown (Figure 3c,e). Together with the findings that the density of microglia was increased upon BDNF knockdown (Figure 2), these

FIGURE 1 BDNF induces the phosphorylation of Trk receptors in microglia. (a) A representative image of a coronal section of an adult mouse brain immunostained for mCherry at 4 weeks after the injection of an AAV encoding the control shRNA. (b) Representative images of the hippocampus immunostained for mCherry and the mossy fiber-specific presynaptic marker SPO. The SL is defined as a thin layer immunostained for SPO. (c) Higher magnification images of the SL shown in (b). (d) Representative images of the SL immunostained for mCherry and proBDNF, a BDNF precursor, in the control shRNA and BDNF shRNA groups. (e) Neuronal BDNF knockdown decreased the intensity of proBDNF staining in the SL. ***$p < .001$, Student's t test; 16 and 17 fields (from two mice) were used for the statistical analysis. (f) A representative image of the hippocampus immunostained for mCherry and the microglial marker Iba1. In the present study, the CA3a region was analyzed. (g) Representative images of the CA3a region immunostained for Iba1 and mCherry. The control shRNA (left panel) and BDNF shRNA (right panel) were used. (h) Representative images of microglia in the CA3 region immunostained for Iba1 and p-Trk. (I) Microglial p-Trk levels were decreased upon neuronal BDNF knockdown. *$p < .05$, Student's t test; 13 and 21 fields (from 2 and 3 mice, respectively) were used for the statistical analysis. (j) Representative images of microglia after saline or KA administration. Samples were immunostained for p-Trk and Iba1. Arrows indicate strong p-Trk signals in microglia. (k) The KA-induced increase in microglial p-Trk levels was blocked by the BDNF shRNA. *$p < .05$ and **$p < .01$, Tukey's test after one-way analysis of variance (ANOVA); 27, 30, and 36 fields (from 3 mice) were used for the statistical analysis. AAV, adeno-associated virus; BDNF, brain-derived neurotrophic factor; DG, dentate gyrus; KA, kainic acid; p-Trk, phosphorylated Trk; proBDNF, pro-brain-derived neurotrophic factor; shRNA, short hairpin RNA; SL, stratum lucidum; SPO, synaptoporin [Color figure can be viewed at wileyonlinelibrary.com]

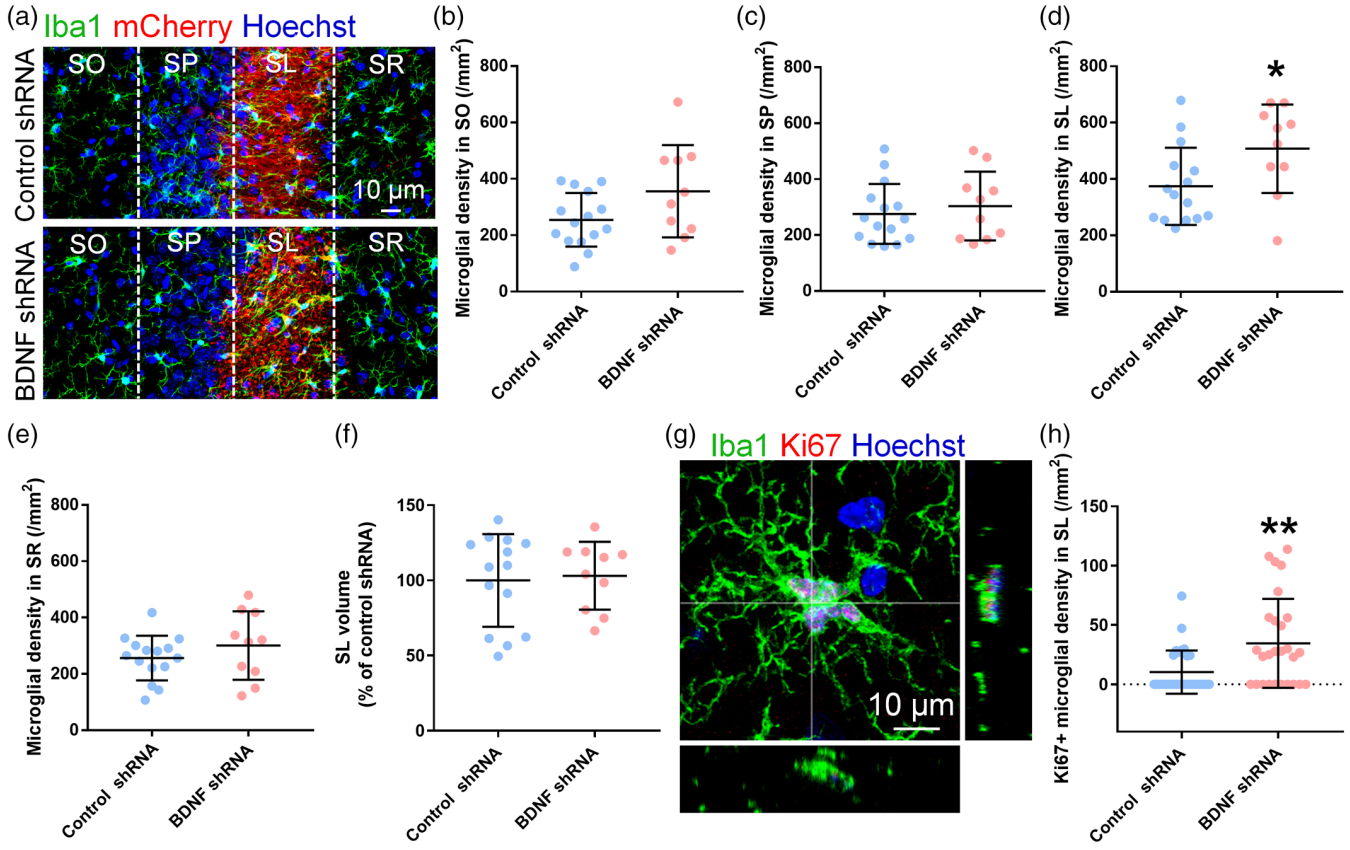

FIGURE 2 Neuronal BDNF knockdown increases the microglial density in the SL at 4 weeks after injection. (a) Representative images of the CA3a region immunostained for Iba1 and mCherry at 4 weeks after AAV injection. (b–e) Neuronal BDNF knockdown increased the microglial density in the SL (d). *$p < .05$, Student's *t* test; 15 and 10 fields (from 4 mice) were used for the statistical analysis. In contrast, neuronal BDNF knockdown did not alter the microglial density in the SO (b), SP (c), or SR (e). $p > .05$, Student's *t* test; 15 and 10 fields (from 4 mice) were used for the statistical analysis. (f) The SL volume was not altered by neuronal BDNF knockdown. $p > .05$, Student's *t* test; 14 and 10 fields (from 4 mice) were included in the statistical analysis. (g) Representative image of microglia in the SL immunostained for Iba1 and Ki67 at 1 week after the AAV injection. (h) Neuronal BDNF knockdown increased the number of Ki67-positive microglia in the SL. **$p < .01$, Student's *t* test; 30 and 27 fields (from 3 mice) were used for the statistical analysis. AAV, adeno-associated virus; BDNF, brain-derived neurotrophic factor; SL, stratum lucidum; SO, stratum oriens; SP, stratum pyramidale; SR, stratum radiatum [Color figure can be viewed at wileyonlinelibrary.com]

data suggest that mossy fiber-derived BDNF prevents microglia from engulfing mossy fiber axons mainly by suppressing the excess proliferation of microglia in the SL.

3.3 | BDNF-Trk signaling modulates the motility of microglial processes and their surveillance area

Microglia rapidly extend and retract their processes and survey their extracellular environment to maintain the homeostasis of neuronal circuits (Davalos et al., 2005; Nimmerjahn, Kirchhoff, & Helmchen, 2005). Microglia continuously contact dendrites and axons with their ramified processes, which has been shown to be associated with spine formation and elimination (Miyamoto et al., 2016). Furthermore, phagocytosis and trogocytosis of neuronal components such as synapses by microglia have been shown to be regulated by the interaction between neurites and microglial processes (Schafer et al., 2012; Weinhard et al., 2018). These findings prompted us to examine the role of BDNF in manipulating the motility of microglial processes. We prepared hippocampal cultures from P10 $CX3CR1^{GFP/+}$ mice in which GFP is expressed in microglia to examine the role of BDNF in microglial motility. We used slice cultures instead of acute slices for the analysis because neuronal injury induced during the preparation of the acute slice itself may induce a transient increase in BDNF expression. The maximal increase in BDNF expression occurs 1–6 hr after traumatic brain injury (TBI) in the hippocampus (Wang et al., 2014). Additionally, we were also concerned about injury-induced acute and abnormal response of microglia during the imaging of acute slices.

We performed time-lapse fluorescence imaging of microglial GFP in slices at 9 DIV (Figure 4a). We confirmed that ramified processes of microglia were visualized with GFP both in live imaging and after immunohistochemistry (Figure 4b). Time-lapse imaging of microglia was performed with or without inhibitors of BDNF signaling, the function blocking antibody anti-BDNF antibody, the Trk inhibitor K252a and the $p75^{NTR}$ inhibitor TAT-Pep5, to examine the role of BDNF signaling in microglial motility. BDNF signaling inhibitors were acutely applied to the medium of the recording chamber, and time-lapse

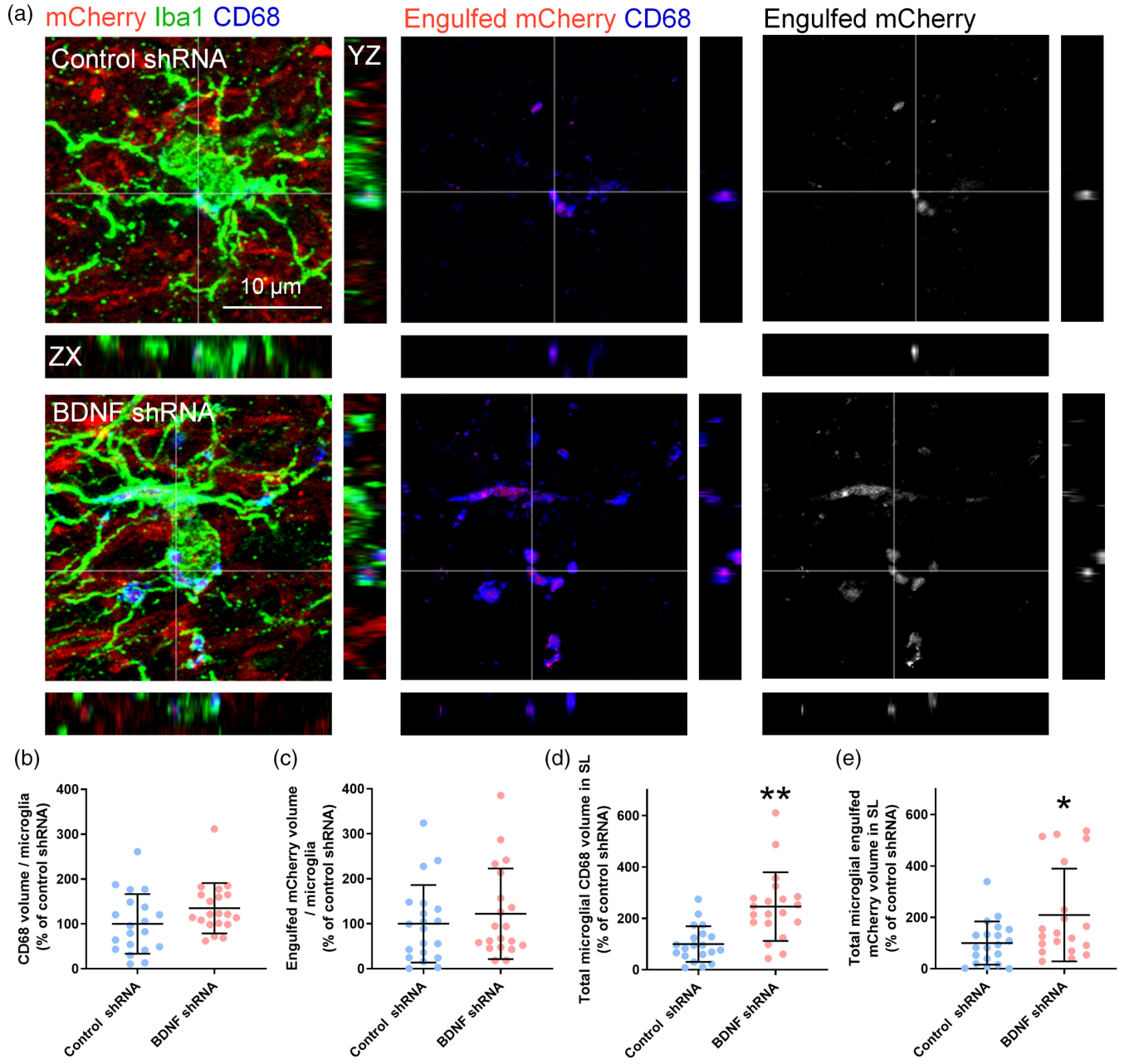

FIGURE 3 Neuronal BDNF knockdown increases the engulfment of axonal components by microglia. (a) Representative *Z*-stack images of microglia in the SL at 4 weeks after AAV injection. Samples were immunostained for Iba1, mCherry, and CD68. We defined mCherry signals incorporated in microglial CD68-positive areas as engulfed axonal components. mCherry engulfed by microglia is shown in the middle and right panels. (b) Neuronal BDNF knockdown did not increase the CD68 volume in the microglial volume. $p > .05$, Student's *t* test; 20 fields (from 4 mice) were used for the statistical analysis. (c) Neuronal BDNF knockdown did not increase the engulfment of mCherry by microglia. $p > .05$, Student's *t* test; 20 fields (from 4 mice) were used for the statistical analysis. (d) Neuronal BDNF knockdown increased the total CD68 volume in microglia in the SL. $^{**}p < .01$, Student's *t* test; 20 fields (from 4 mice) were used for the statistical analysis. (e) Neuronal BDNF knockdown increased the total volume of mCherry engulfed in microglia in the SL. $^{*}p < .05$, Student's *t* test; 20 fields (from 4 mice) were used for the statistical analysis. AAV, adeno-associated virus; BNDF, brain-derived neurotrophic factor; SL, stratum lucidum [Color figure can be viewed at wileyonlinelibrary.com]

imaging of microglia was performed immediately after the application of BDNF signaling inhibitors at 9 DIV. Microglia in the SL were observed, and the process length was measured every minute for 10 min (Figure 4) and the surveillance area was measured every minute for 30 min (Figure 5).

The length of the microglial process was defined as the distance between the point at which the process emanated from the soma and the tip of the process after applying the threshold to GFP signals (Figure 4c). The anti-BDNF ab and K252a increased both the extension speed (Figure 4d) and contraction speed (Figure 4e). Based on

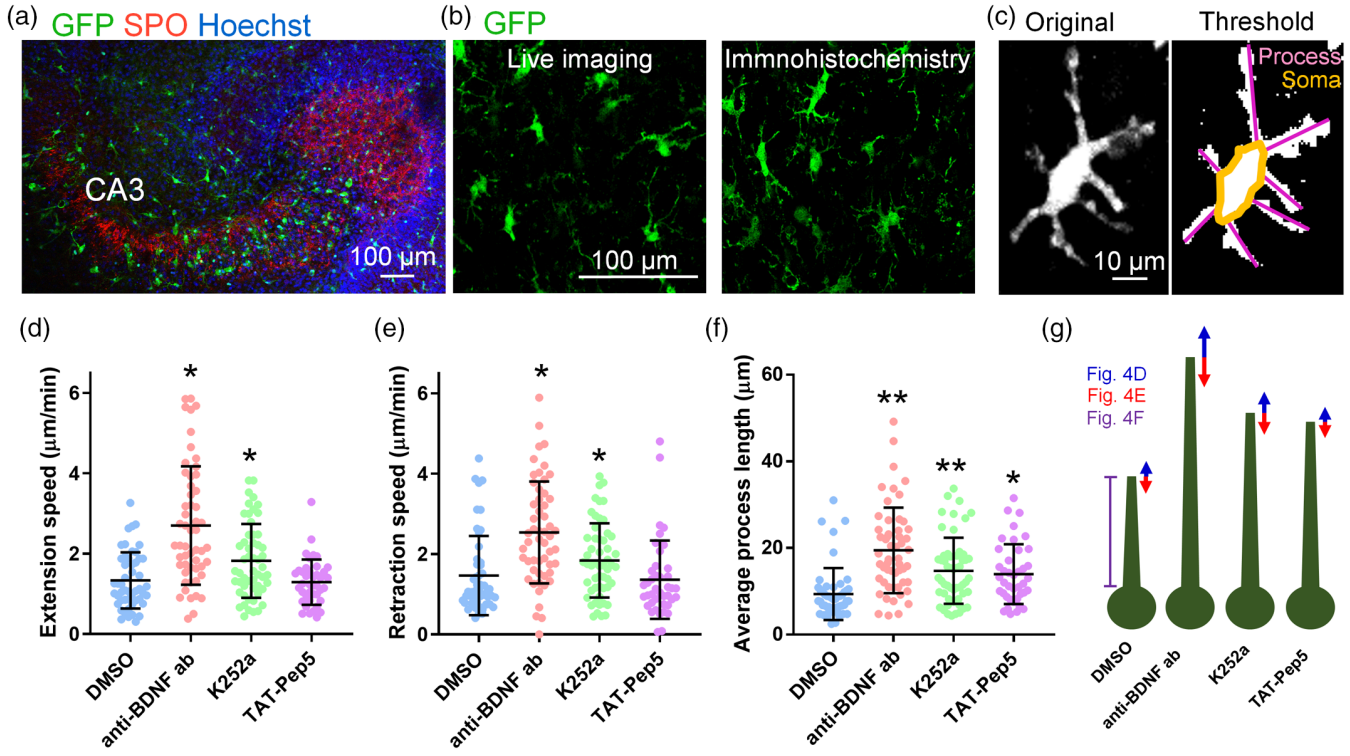

FIGURE 4 The inhibition of BDNF-Trk signaling increases the motility of microglial processes. (a) A representative image of a cultured hippocampal slice prepared from a P10 CX3CR1$^{GFP/+}$ mouse that was immunostained for GFP and SPO at 9 DIV. (b) Left panel—A representative image of GFP-positive microglia in a cultured hippocampal slice during a live imaging session at 9 DIV. Right panel—A representative image of GFP-positive microglia in the SL from a cultured hippocampal slice at 9 DIV. (c) Left panel—A representative image of microglia during a live imaging session. Right panel—A thresholded image of the left panel for the analysis of process motility. The orange circle indicates the microglial soma, and purple lines connect the tip of the process and the point at which the process emanates from the soma. The length of the purple line is defined as the length of the process. (d,e) The addition of anti-BDNF or K252a increased the average process length and contraction speed. $^{*}p < .05$ compared with DMSO, Dunn's test after one-way analysis of variance (ANOVA); 50, 54, 54, and 41 processes were subjected to the statistical analysis, and these processes were obtained from 3, 3, 4, and 4 slices, respectively. (f) The addition of anti-BDNF or K252a increased the average process length. $^{**}p < .01$ compared with DMSO, Dunn's test after one-way ANOVA; 67, 79, 80, and 62 processes were statistically analyzed, and these processes were obtained from 3, 3, 4, and 4 slices, respectively. (g) Schematic summarizing the results presented in Figure 4d–f. 9 DIV, ninth day in vitro; BDNF, brain-derived neurotrophic factor; DG, dentate gyrus; DMSO, dimethyl sulfoxide; GFP, green fluorescent protein; P10, postnatal Day 10; SL, stratum lucidum; SPO, synaptoporin [Color figure can be viewed at wileyonlinelibrary.com]

our data, the average extension and retraction speeds (means ± *SEM*) were 1.33 ± 0.10 μm/min (Figure 4d) and 1.46 ± 0.14 μm/min (Figure 4e), respectively, consistent with previous in vivo studies. Nimmerjahn et al. reported average extension and retraction speeds of 1.47 ± 0.10 μm/min and 1.47 ± 0.08 μm/min in vivo (Nimmerjahn et al., 2005), respectively. In addition, Gyoneva et al. reported baseline microglial process dynamics of 1.01 ± 0.026 μm/min (Gyoneva et al., 2014). In acute slices, the average velocity of the tips of individual microglial processes was 2.38 ± 0.08 μm/min in a previous study (Avignone, Lepleux, Angibaud, & Nägerl, 2015). Thus, our data are generally consistent with the results obtained in vivo in terms of the speed of microglial processes. Furthermore, the average length of the microglial process was increased by the anti-BDNF ab, K252a, and TAT-Pep5 (Figure 4b,f). Thus, BDNF signaling likely suppresses the motility and average length of microglial processes in slice cultures (Figure 4g).

We also investigated whether the inhibition of BDNF signaling affects the area surveyed by microglial processes. Surveillance area expansion and retraction were defined as areas where the GFP signal appeared or disappeared, respectively, compared with the image captured in the previous minute. The average changes in the values of these two parameters (extension and retraction) were increased by the application of either the anti-BDNF ab or K252a (Figure 5a–c).

Additionally, we defined total surveillance area as the area where the GFP signal appeared or disappeared even once within 30 min (images were captured every minute). Pseudocolor images of the total surveillance area are shown in Figure 5d. The total surveillance area was increased by the anti-BDNF ab and K252a (Figure 5e). Based on these results, BDNF signaling likely reduces the areas explored by microglial processes in slice cultures.

3.4 | BDNF-Trk signaling protects synapses from engulfment by microglia

An increase in the surveillance area may have facilitated neuron–microglial interactions, including the phagocytosis of synapses by

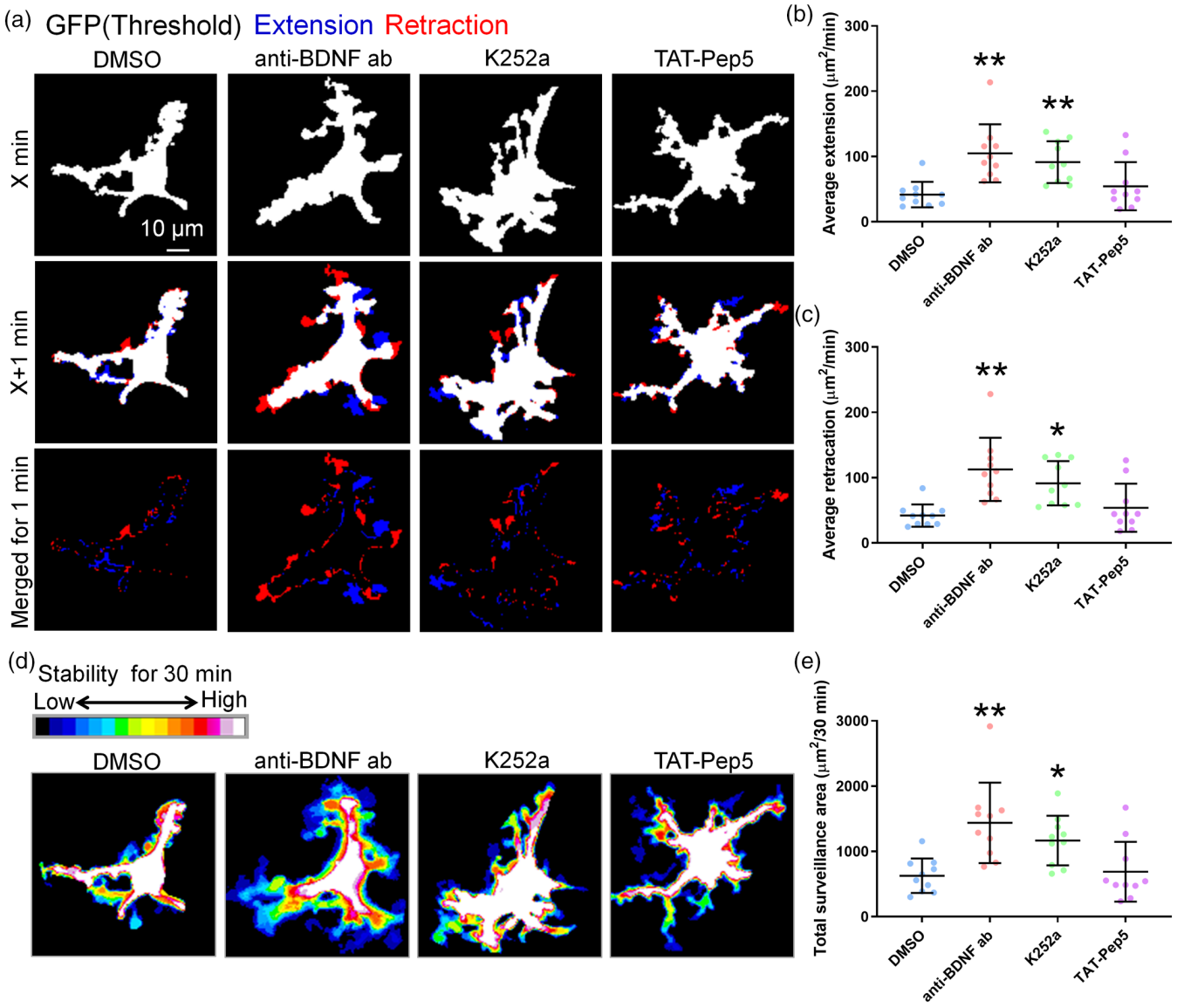

FIGURE 5 BDNF-Trk signaling inhibitors increased the microglial surveillance area. (a) Representative images of GFP-positive microglia in slice cultures to which threshold was applied at X min in live imaging sessions. Blue and red areas indicate extension and retraction surveillance areas, respectively. Merged extension and retraction surveillance areas at 1 min and 30 min are shown. (b) The anti-BDNF ab and K252a increased the extension surveillance area. $^{**}p < .01$ compared with DMSO, Dunnett's test after one-way analysis of variance (ANOVA); 10 microglial cells were included in the statistical analysis, and these cells were obtained from 3 slices. (c) The anti-BDNF ab and K252a increased the retraction surveillance area. $^{*}p < .05$ and $^{**}p < .01$ compared with DMSO, Dunnett's test after one-way ANOVA; 10 microglial cells were included in the statistical analysis, and these cells were obtained from 3 slices. (d) Representative pseudocolor images of microglial stability based on the GFP signal frequency within 30 min. (e) The anti-BDNF ab and K252a increased the total surveillance area within 30 min. $^{*}p < .05$ and $^{**}p < .01$ compared with DMSO, Dunnett's test after one-way ANOVA; 10 microglial cells were statistically analyzed, and these cells were obtained from 3 slices. BDNF, brain-derived neurotrophic factor; DMSO, dimethyl sulfoxide; GFP, green fluorescent protein; SL, stratum lucidum [Color figure can be viewed at wileyonlinelibrary.com]

microglia. Next, we investigated whether the inhibition of BDNF signaling altered synaptic engulfment by microglia in the SL. One day after the addition of BDNF signaling inhibitors at 9 DIV, we immunohistochemically assessed the volume of SPO that was engulfed in microglial lysosomes ($CD68^{+}$) (Figure 6a). The CD68 volume in the microglia was increased by the anti-BDNF ab (Figure 6b). In addition, the total CD68 volume in the SL was increased by either the anti-BDNF ab or K252a (Figure 6c). Therefore, BDNF-Trk signaling suppresses the phagocytic activity of microglia. Furthermore, both the volume of SPO engulfed in the microglial volume (Figure 6d) and the total volume of SPO engulfed by microglia in the SL (Figure 6e) were increased by the anti-BDNF ab and K252a. Additionally, the $p75^{NTR}$ inhibitor TAT-Pep5 and heat-inactivated anti-BDNF antibody did not alter the lysosomal volume nor synaptic engulfment by microglia (Figure 6b–e). Thus, BDNF-Trk signaling, but not BDNF-$p75^{NTR}$ signaling,

prevents excess microglial engulfment of mossy fiber synapses. We also confirmed that inhibitors of BDNF signaling increased the microglial density in the SL but did not alter the SL volume (Figure S4), consistent with the data obtained using the BDNF shRNA in vivo (Figure 2d,f).

4 | DISCUSSION

Microglia play key roles in the development and maintenance of neuronal circuits during development and in adulthood. Microglia and neurons interact via soluble and contact-dependent factors (Wohleb,

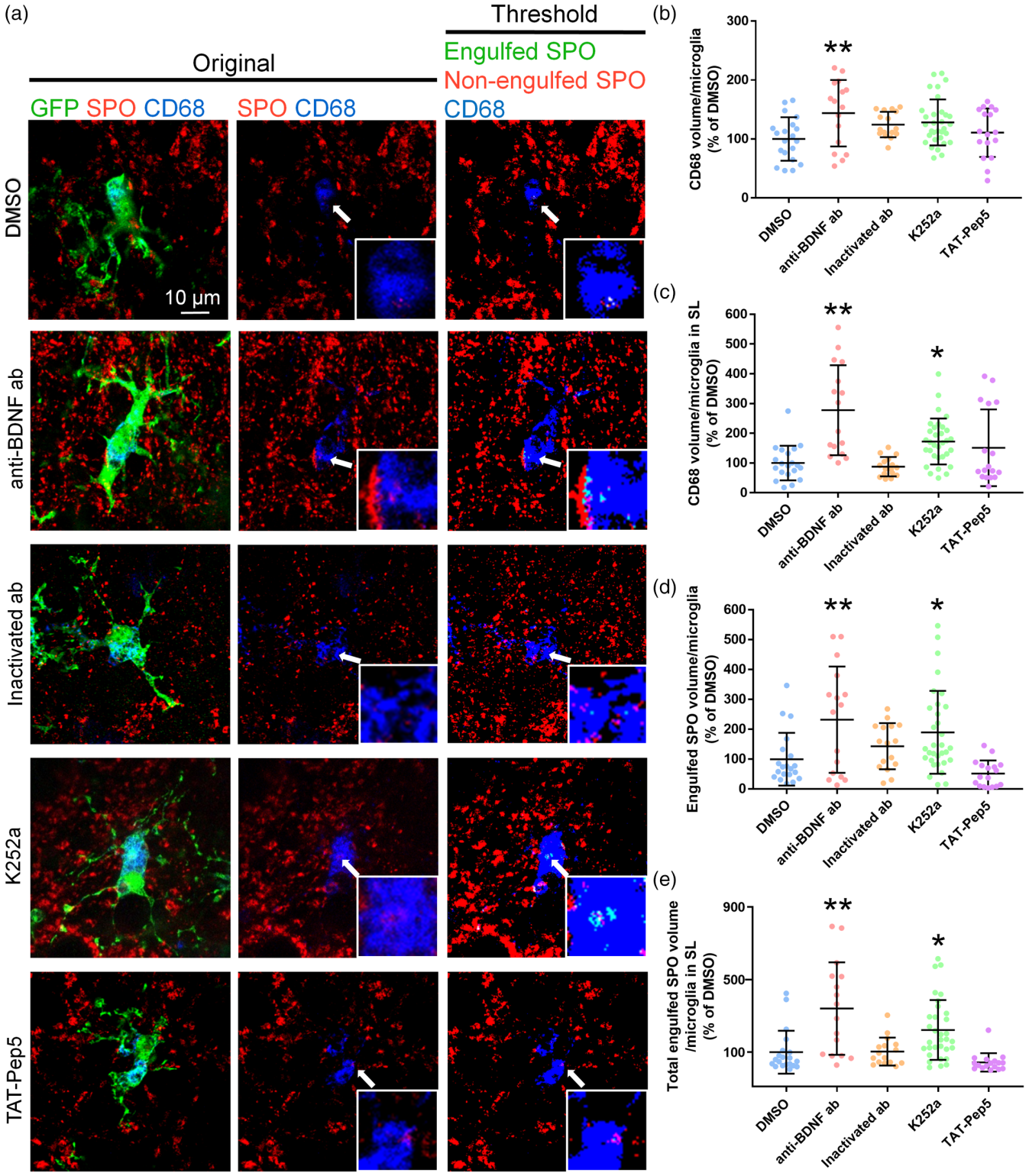

FIGURE 6 Legend on next page.

2016). However, the molecular mechanisms that modulate neuron–microglia interactions remain to be fully elucidated. Specifically, researchers have not yet determined whether neuronal BDNF, a major neurotrophic factor, affects microglial dynamics. Here, we propose the possibility that neuronal BDNF plays a role in suppressing the engulfment of axonal components by microglia in the hippocampus. Notably, shRNA-mediated BDNF knockdown in dentate granule cells resulted in an increased microglial density and increased engulfment of axonal components in the SL where dentate granule cells project their axons. Additionally, inhibition of the BDNF signaling pathway increased microglial dynamics and the engulfment of presynaptic structures.

Based on the findings from the present study, we conclude that neuronal BDNF modulates microglial dynamics. However, further studies are required to completely elucidate the underlying molecular mechanisms. We postulate that neuronal BDNF affects microglia through both direct and indirect mechanisms.

First, neuronal BDNF may directly activate BDNF receptors expressed on microglia. Does neuronal BDNF released into the extracellular space reach microglia? Based on a previous study, we assume that released BDNF is detectable at a minimum distance of 4.5 μm from synapses because the study reported that an endogenous BDNF source must be located within 4.5 μm of synapses to induce dendritic plasticity (Horch & Katz, 2002). This range would allow microglia to sense neuronal BDNF, as microglia frequently contact synapses under physiological conditions. In addition, kainic acid, which is known to enhance the activity-dependent release of neuronal BDNF, increased p-Trk levels in microglia, a phenomenon that was blocked by knocking down neuronal BDNF (Figure 1j,k). Therefore, BDNF released from mossy fiber boutons likely directly activates microglial TrkB in the hippocampus. Furthermore, Mizoguchi et al. (2014) reported that exogenous BDNF activated truncated TrkB in cultured microglia, resulting in the sustained elevation of intercellular Ca^{2+} concentrations in microglia. Therefore, the hypothesis that BDNF receptors on microglial processes are directly activated by neuronal BDNF is plausible.

Second, neuronal BDNF may also indirectly affect microglial dynamics because in addition to neurons and microglia, astrocytes express TrkB (Aroeira, Sebastião, & Valente, 2015). Because astrocytes release ATP, which has been shown to serve as an attractant for microglial processes and microglia themselves, inhibition of the BDNF signaling pathway in astrocytes indirectly affects microglial dynamics via purinergic signaling (Anderson, Bergher, & Swanson, 2004). Thus, our observations may be related to multiple direct (on microglia) and indirect (on cells other than microglia) effects of BDNF.

In the current study, knockdown of neuronal BDNF increased the microglial density in the SL 4 weeks after the virus injection (Figure 2d). The local microglial density is increased though migration and/or proliferation when neuronal circuit homeostasis is needed. Luo, Koyama, and Ikegaya (2016) reported increased microglial proliferation in the dentate gyrus after status epilepticus for the engulfment of excess newborn neurons. According to Kurpius, Nolley, and Dailey (2007), microglial migration toward hippocampal neurons is facilitated by traumatic neuronal injury for the purpose of eliminating injured cells.

In the present study, microglial proliferation induced by the knockdown of neuronal BDNF partially contributed to an increase in the microglial density (Figure 2g,h). In contrast, the microglial density in the areas adjacent to SL was not changed by BDNF knockdown (Figure 2b–e). However, we postulate that these data do not necessarily indicate a lack of change in microglial migration because microglia maintain their density in local areas through migration and proliferation (Zhan et al., 2019). Microglial migration would be accompanied by a temporary decrease in the microglial density in areas where they were originally located. However, the decrease may be immediately buffered by the migration of microglia from adjacent areas and microglial proliferation. Long-term time-lapse (continuous 2-day) imaging of microglia in the slice cultures might have helped us examine proliferation or cell mobility, but the extensive cell damage induced by the procedure prevented us from performing these experiments. Therefore, further studies are needed to determine whether microglial migration is induced by knocking down neuronal BDNF.

Moreover, BDNF knockdown increased the amount of mossy fibers engulfed by microglia in the SL at 4 weeks after virus injection (Figure 3e). Because the amount of neuronal processes engulfed by microglia was not significantly different (Figure 3c), the increase in

FIGURE 6 The inhibition of BDNF-Trk signaling increases the engulfment of presynaptic structures by microglia. (a) Representative *Z*-stack images of microglia in the SL from cultured hippocampal slices at 10 DIV were captured 1 day after the addition of a BDNF signaling inhibitor. The left and middle panels show original images of samples immunostained for GFP, SPO, and CD68. Right panels show the thresholded images of the original data. SPO signals in the CD68-positive portions of microglia were defined as engulfed SPO (green). The image within the square in each panel is a higher magnification image of the area indicated by arrows. (b) The addition of the anti-BDNF ab increased the CD68 volume in the microglial volume. $^{**}p < .01$ compared with DMSO, Dunnett's test after one-way analysis of variance (ANOVA). Then, 20, 16, 16, 32, and 21 fields (from 9, 7, 7, 13, and 9 slices, respectively) were statistically analyzed. (c) The addition of the anti-BDNF ab or K252a increased the total CD68 volume in microglia in the SL. $^{*}p < .05$ and $^{**}p < .001$ compared with DMSO, Dunnett's test after one-way ANOVA. Also, 20, 16, 16, 32, and 21 fields (from 9, 7, 7, 13, and 9 slices, respectively) were used subjected to statistical analyses. (d) The application of the anti-BDNF or K252a increased the volume of engulfed SPO in the microglial volume. $^{*}p < .05$ and $^{**}p < .01$ compared with DMSO, Dunnett's test after one-way ANOVA. Then, 20, 16, 16, 32, and 21 fields (from 9, 7, 7, 13, and 9 slices, respectively) were subjected to the statistical analysis. (e) The addition of the anti-BDNF or K252a increased the total volume of engulfed SPO in the SL. $^{*}p < .05$ and $^{**}p < .01$ compared with DMSO, Dunnett's test after one-way ANOVA. Also 20, 16, 16, 32, and 21 fields (from 9, 7, 7, 13, and 9 slices, respectively) were statistically analyzed. 10 DIV, 10th day in vitro; BDNF, brain-derived neurotrophic factor; DMSO, dimethyl sulfoxide; GFP, green fluorescent protein; SL, stratum lucidum; SPO, synaptoporin [Color figure can be viewed at wileyonlinelibrary.com]

microglial density mainly contributed to the increase in the total amount of engulfed mossy fibers in the SL. Inhibitors of BDNF signaling enhanced phagocytic activity of microglia in vitro (Figure 6d), whereas the BDNF shRNA did not significantly enhance phagocytic activity of microglia in vivo (Figure 3c). We assume that this discrepancy is partially attributed to the difference in the method used to suppress BDNF signaling: direct application of BDNF signaling inhibitors in vitro vs. a BDNF shRNA in vivo. The BDNF shRNA decreased BDNF levels, which were detected by the measuring the immunoreactivity of the proBDNF protein, in the SL to 69.05% (control shRNA, 100.00 ± 8.05%; BDNF shRNA, 69.05 ± 3.16%) of the sample injected with the control shRNA (Figure 1(d,e). As shown in our previous study, 1.6 μg/ml anti-BDNF antibody or 0.3 μM K252a significantly inhibited BDNF signaling-induced phenomena, that is, mossy fiber sprouting, in hippocampal slice cultures in which the expression of BDNF protein was increased by at least 10 times by picrotoxin compared to the control (Koyama et al., 2004). Therefore, we suspect that the application of BDNF inhibitors more efficiently inhibited BDNF signaling than the BDNF shRNA. Another possible explanation for the difference in the phagocytic activity of microglia is the difference between the phenotype of microglia in organotypic cultures and in vivo (Masuch et al., 2016). In the present study, the microglial morphologies shown in Figure 1 (in vivo) and Figure 4 (slice culture) differed.

The AAVs used in our study silenced the expression of both BDNF and proBDNF, a precursor of BDNF that is a ligand of $p75^{NTR}$. In addition, BDNF itself is a low-affinity ligand for $p75^{NTR}$. Therefore, our in vivo results reflect the inactivation of both the TrkB and $p75^{NTR}$ pathways. However, our in vitro experiments showed increases in the microglial process speed, surveillance area and the engulfment of presynaptic structures by microglia following treatment with the Trk inhibitor K252a, but not the $p75^{NTR}$ inhibitor TAT-Pep5, while the microglial density was increased after treatment with either K252a or TAT-Pep5 (Figures 4–6 and S4). Thus, we propose that neuronal BDNF-microglial Trk signaling plays an important role in the mechanism regulating microglial density and the engulfment of axons in vivo.

The frequency of neuron–microglia interactions mediated by neuronal BDNF depends on the expression and release of BDNF, which are potentially affected by multiple factors, including BDNF polymorphisms. For example, the BDNF Val66 Met allele (met-BDNF) decreases the activity-dependent release of BDNF from hippocampal neurons, while the neuronal expression of BDNF is unchanged (Egan et al., 2003). In a recent study using a mouse model of TBI, the expression of the met-BDNF allele disrupted BDNF signaling and promoted microglial activation in the hippocampus (Giarratana et al., 2019). Moreover, in the TBI model, AAV-mediated overexpression of wild-type neuronal BDNF resulted in increased p-Trk levels in the hippocampus and ameliorated cognitive deficits. Thus, the BDNF-mediated manipulation of microglial dynamics potentially represents a novel therapeutic strategy for brain diseases in which neuron–microglia interactions play a crucial role, such as TBI.

Further studies are needed to determine whether neuronal BDNF modulates neuron–microglia interactions in other brain regions and whether it affects brain function and behaviors. The brain region-specific heterogeneity of microglia should also be considered when examining this mechanism (Yang et al., 2013).

ACKNOWLEDGMENTS

This study was partially supported by a Grant-in-Aid for Scientific Research (B) (17H03988 to R. K.) from JSPS, JST PRESTO (JPMJPR18H4 to R. K.), and JST ERATO (JPMJER1801 to Y. I.).

CONFLICT OF INTEREST

The authors declare no conflicts of interest.

DATA AVAILABILITY STATEMENT

All data needed to evaluate the conclusions described in the paper are presented in the paper and the Supplementary Materials. The additional data that support the findings of this study are available from the corresponding author upon reasonable request.

ORCID

Ryuta Koyama https://orcid.org/0000-0001-7108-174X

REFERENCES

Anderson, C. M., Bergher, J. P., & Swanson, R. A. (2004). ATP-induced ATP release from astrocytes. *Journal of Neurochemistry*, *88*(1), 246–256.

Andoh, M., Shibata, K., Okamoto, K., Onodera, J., Morishita, K., Miura, Y., … Koyama, R. (2019). Exercise reverses behavioral and synaptic abnormalities after maternal inflammation. *Cell Reports*, *27*(10), 2817–2825.

Aroeira, R. I., Sebastião, A. M., & Valente, C. A. (2015). BDNF, via truncated TrkB receptor, modulates GlyT1 and GlyT2 in astrocytes. *Glia*, *63*, 2181–2197.

Avignone, E., Lepleux, M., Angibaud, J., & Nägerl, U. V. (2015). Altered morphological dynamics of activated microglia after induction of status epilepticus. *Journal of Neuroinflammation*, *12*, 202.

Conner, J. M., Lauterborn, J. C., Yan, Q., Gall, C. M., & Varon, S. (1997). Distribution of brain-derived neurotrophic factor (BDNF) protein and mRNA in the normal adult rat CNS: Evidence for anterograde axonal transport. *The Journal of Neuroscience*, *17*(7), 2295–2313.

Coull, J. A., Beggs, S., Boudreau, D., Boivin, D., Tsuda, M., Inoue, K., … de Koninck, Y. (2005). BDNF from microglia causes the shift in neuronal anion gradient underlying neuropathic pain. *Nature*, *438*(7070), 1017–1021.

Crozier, R. A., Bi, C., Han, Y. R., & Plummer, M. R. (2008). BDNF modulation of NMDA receptors is activity dependent. *Journal of Neurophysiology*, *100*(6), 3264–3274.

Danzer, S. C., & McNamara, J. O. (2004). Localization of brain-derived neurotrophic factor to distinct terminals of mossy fiber axons implies regulation of both excitation and feedforward inhibition of CA3 pyramidal cells. *The Journal of Neuroscience.*, *24*(50), 11346–11355.

Davalos, D., Grutzendler, J., Yang, G., Kim, J. V., Zuo, Y., Jung, S., … Gan, W. B. (2005). ATP mediates rapid microglial response to local brain injury in vivo. *Nature Neuroscience*, *8*(6), 752–758.

Ding, H., Chen, J., Su, M., Lin, Z., Zhan, H., Yang, F., … Zhou, X. (2020). BDNF promotes activation of astrocytes and microglia contributing to neuroinflammation and mechanical allodynia in cyclophosphamide-induced cystitis. *Journal of Neuroinflammation*, *17*(1), 19.

Duman, R. S., & Monteggia, L. M. (2006). A neurotrophic model for stress-related mood disorders. *Biological Psychiatry*, *59*(12), 1116–1127.

Egan, M. F., Kojima, M., Callicott, J. H., Goldberg, T. E., Kolachana, B. S., Bertolino, A., … Weinberger, D. R. (2003). The BDNF val66met

polymorphism affects activity-dependent secretion of BDNF and human memory and hippocampal function. *Cell*, *112*(2), 257–269.

Falcicchia, C., Trempat, P., Binaschi, A., Perrier-Biollay, C., Roncon, P., Soukupova, M., … Simonato, M. (2016). Silencing status epilepticus-induced BDNF expression with herpes simplex virus type-1 based amplicon vectors. *PLoS One*, *11*(3), e0150995.

Ferrini, F., & de Koninck, Y. (2013). Microglia control neuronal network excitability via BDNF signalling. *Neural Plasticity*, *2013*, 429815.

Frisen, J., Verge, V. M., Fried, K., Risling, M., Persson, H., Trotter, J., … Lindholm, D. (1993). Characterization of glial trkB receptors: Differential response to injury in the central and peripheral nervous systems. *Proceedings of the National Academy of Sciences of the United States of America*, *90*, 4971–4975.

Giarratana, A. O., Teng, S., Reddi, S., Zheng, C., Adler, D., Thakker-Varia, S., & Alder, J. (2019). BDNF Val66Met genetic polymorphism results in poor recovery following repeated mild traumatic brain injury in a mouse model and treatment with AAV-BDNF improves outcomes. *Frontiers in Neurology*, *10*, 1175.

Gyoneva, S., Davalos, D., Biswas, D., Swanger, S. A., Garnier-Amblard, E., Loth, F., … Traynelis, S. F. (2014). Systemic inflammation regulates microglial responses to tissue damage in vivo. *Glia*, *62*(8), 1345–1360.

Helgager, J., Liu, G., & McNamara, J. O. (2013). The cellular and synaptic location of activated TrkB in mouse hippocampus during limbic epileptogenesis. *The Journal of Comparative Neurology*, *521*(3), 499–521.

Hiragi, T., Ikegaya, Y., & Koyama, R. (2018). Microglia after seizures and in epilepsy. *Cells*, *7*(4), 26.

Horch, H. W., & Katz, L. C. (2002). BDNF release from single cells elicits local dendritic growth in nearby neurons. *Nature Neuroscience*, *5*(11), 1177–1184.

Korte, M., Carroll, P., Wolf, E., Brem, G., Thoenen, H., & Bonhoeffer, T. (1995). Hippocampal long-term potentiation is impaired in mice lacking brain-derived neurotrophic factor. *Proceedings of the National Academy of Sciences of the United States of America*, *92*(19), 8856–8860.

Koyama, R., Muramatsu, R., Sasaki, T., Kimura, R., Ueyama, C., Tamura, M., … Ikegaya, Y. (2007). A low-cost method for brain slice cultures. *Journal of Pharmacological Sciences*, *104*(2), 191–194.

Koyama, R., Yamada, M. K., Fujisawa, S., Katoh-Semba, R., Matsuki, N., & Ikegaya, Y. (2004). Brain-derived neurotrophic factor induces hyperexcitable reentrant circuits in the dentate gyrus. *The Journal of Neuroscience*, *24*(33), 7215–7224.

Kurpius, D., Nolley, E. P., & Dailey, M. E. (2007). Purines induce directed migration and rapid homing of microglia to injured pyramidal neurons in developing hippocampus. *Glia*, *55*(8), 873–884.

Li, Y., Calfa, G., Inoue, T., Amaral, M. D., & Pozzo-Miller, L. (2010). Activity-dependent release of endogenous BDNF from mossy fibers evokes a TRPC3 current and Ca2+ elevations in CA3 pyramidal neurons. *Journal of Neurophysiology*, *103*(5), 2846–2856.

Lindholm, D., Carroll, P., Tzimagiorgis, G., & Thoenen, H. (1996). Autocrine-paracrine regulation of hippocampal neuron survival by IGF-1 and the neurotrophins BDNF, NT-3 and NT-4. *The European Journal of Neuroscience*, *8*(7), 1452–1460.

Lübke, J., Frotscher, M., & Spruston, N. (1998). Specialized electrophysiological properties of anatomically identified neurons in the hilar region of the rat fascia dentata. *Journal of Neurophysiology*, *79*(3), 1518–1534.

Luo, C., Koyama, R., & Ikegaya, Y. (2016). Microglia engulf viable newborn cells in the epileptic dentate gyrus. *Glia*, *64*(9), 1508–1517.

Madry, C., & Attwell, D. (2015). Receptors, ion channels, and signaling mechanisms underlying microglial dynamics. *The Journal of Biological Chemistry*, *290*(20), 12443–12450.

Masuch, A., van der Pijl, R., Füner, L., Wolf, Y., Eggen, B., Boddeke, E., & Biber, K. (2016). Microglia replenished OHSC: A culture system to study in vivo like adult microglia. *Glia*, *64*(8), 1285–1297.

Matsushita, T., Elliger, S., Elliger, C., Podsakoff, G., Villarreal, L., Kurtzman, G. J., … Colosi, P. (1998). Adeno-associated virus vectors can be efficiently produced without helper virus. *Gene Therapy*, *5*, 938–945.

Ménard, C., Hodes, G. E., & Russo, S. J. (2016). Pathogenesis of depression: Insights from human and rodent studies. *Neuroscience*, *321*, 138–162.

Miyamoto, A., Wake, H., Ishikawa, A. W., Eto, K., Shibata, K., Murakoshi, H., … Nabekura, J. (2016). Microglia contact induces synapse formation in developing somatosensory cortex. *Nature Communications*, *7*, 12540.

Mizoguchi, Y., Kato, T. A., Seki, Y., Ohgidani, M., Sagata, N., Horikawa, H., … Monji, A. (2014). Brain-derived neurotrophic factor (BDNF) induces sustained intracellular Ca2+ elevation through the up-regulation of surface transient receptor potential 3 (TRPC3) channels in rodent microglia. *The Journal of Biological Chemistry*, *289*(26), 18549–18555.

Murray, K. D., Isackson, P. J., Eskin, T. A., King, M. A., Montesinos, S. P., Abraham, L. A., & Roper, S. N. (2000). Altered mRNA expression for brain-derived neurotrophic factor and type II calcium/calmodulin-dependent protein kinase in the hippocampus of patients with intractable temporal lobe epilepsy. *The Journal of Comparative Neurology*, *418*(4), 411–422.

Nimmerjahn, A., Kirchhoff, F., & Helmchen, F. (2005). Resting microglial cells are highly dynamic surveillants of brain parenchyma in vivo. *Science*, *308*(5726), 1314–1318.

Palomer, E., Carretero, J., Benveqnu, S., Dotti, C. G., & Martin, M. G. (2016). Neuronal activity controls Bdnf expression via polycomb de-repression and CREB/CBP/JMJD3 activation in mature neurons. *Nature Communications*, *7*, 11081.

Parkhurst, C. N., Yang, G., Ninan, I., Savas, J. N., Yates, J. R., III, Lafaille, J. J., … Gan, W. B. (2013). Microglia promote learning-dependent synapse formation through brain-derived neurotrophic factor. *Cell*, *155*(7), 1596–1609.

Perego, C., Fumagalli, S., & de Simoni, M. G. (2011). Temporal pattern of expression and colocalization of microglia/macrophage phenotype markers following brain ischemic injury in mice. *Journal of Neuroinflammation*, *8*, 174.

Racine, R. J. (1972). Modification of seizure activity by electrical stimulation. II. Motor seizure. *Electroencephalography and Clinical Neurophysiology*, *32*(3), 281–294.

Samad, O. A., Tan, A. M., Cheng, X., Foster, E., Dib-Hajj, S. D., & Waxman, S. G. (2013). Virus-mediated shRNA knockdown of Na(v)1.3 in rat dorsal root ganglion attenuates nerve injury-induced neuropathic pain. *Molecular Therapy*, *21*(1), 49–56.

Schafer, D. P., Lehrman, E. K., Kautzman, A. G., Koyama, R., Mardinly, A. R., Yamasaki, R., … Stevens, B. (2012). Microglia sculpt postnatal neural circuits in an activity and complement-dependent manner. *Neuron*, *74*(4), 691–705.

Takahashi, M., Hayashi, S., Kakita, A., Wakabayashi, K., Fukuda, M., Kameyama, S., … Nawa, H. (1999). Patients with temporal lobe epilepsy show an increase in brain-derived neurotrophic factor protein and its correlation with neuropeptide Y. *Brain Research*, *818*(2), 579–582.

Wang, L., Chang, X., She, L., Xu, D., Huang, W., & Poo, M. M. (2015). Autocrine action of BDNF on dendrite development of adult-born hippocampal neurons. *The Journal of Neuroscience*, *35*(22), 8384–8393.

Wang, Y., Hameed, M. Q., Rakhade, S. N., Iglesias, A. H., Muller, P. A., Mou, D. L., & Rotenberg, A. (2014). Hippocampal immediate early gene transcription in the rat fluid percussion traumatic brain injury model. *Neuroreport*, *25*(12), 954–959.

Weinhard, L., di Bartolomei, G., Bolasco, G., Machado, P., Schieber, N. L., Neniskyte, U., … Gross, C. T. (2018). Microglia remodel synapses by presynaptic trogocytosis and spine head filopodia induction. *Nature Communications*, *9*(1), 1228.

Williams, M. E., Wilke, S. A., Daggett, A., Davis, E., Otto, S., Ravi, D., … Ghosh, A. (2011). Cadherin-9 regulates synapse-specific differentiation in the developing hippocampus. *Neuron*, *71*(4), 640–655.

Wohleb, E. S. (2016). Neuron-microglia interactions in mental health disorders: "For better, and for worse". *Frontiers in Immunology*, *7*, 544.

Yang, T. T., Lin, C., Hsu, C. T., Wang, T. F., Ke, F. Y., & Kuo, Y. M. (2013). Differential distribution and activation of microglia in the brain of male C57BL/6J mice. *Brain Structure & Function*, *218*(4), 1051–1060.

Zhan, L., Krabbe, G., Du, F., Jones, I., Reichert, M. C., Telpoukhovskaia, M., … Gan, L. (2019). Proximal recolonization by self-renewing microglia re-establishes microglial homeostasis in the adult mouse brain. *PLoS Biology*, *17*(2), e3000134.

Zhang, J., Geula, C., Lu, C., Koziel, H., Hatcher, L. M., & Roisen, F. J. (2003). Neurotrophins regulate proliferation and survival of two microglial cell lines in vitro. *Experimental Neurology*, *183*(2), 469–481.

SUPPORTING INFORMATION

Additional supporting information may be found online in the Supporting Information section at the end of this article.

How to cite this article: Onodera J, Nagata H, Nakashima A, Ikegaya Y, Koyama R. Neuronal brain-derived neurotrophic factor manipulates microglial dynamics. *Glia*. 2021;69: 890–904. https://doi.org/10.1002/glia.23934